

Research/Technical Note

Study of Octupole Transitions in Xe, Ba, Ce and Nd Nuclei within Interacting Boson Model

Tuqa Abdulbaset Hashim, Saad Naji Abood*

Physics Department, College of Sciences, AL-Nahrain University, Baghdad, Iraq

Abstract

For nuclei with $54 \leq Z \leq 60$ and $86 \leq N \leq 94$, the results regarding the excitation spectra at low energies, both in positive and negative parity, as well as the transition probabilities for electric dipole (B(E1)), quadrupole (B(E2)), and octupole transitions (B(E3)), indicate the emergence of significant octupole behavior. These observations have been made using the Interacting Boson Model-1 (IBM-1). The study examines the onset of octupole deformation and its impact on the spectroscopic characteristics in even-even neutron-rich lanthanide isotopes, specifically in the Ba and Nd nuclei. The investigation compares the results obtained from the Interacting Boson Model-1 (IBM-1) with the existing experimental data. The focus is on understanding how the addition of neutrons influences the development of octupole deformation and its manifestation in the observed spectroscopic features. The onset of strong octupolarity for $Z \approx 56$ and $N \approx 88$ nuclei is indicated by the results obtained for the electric dipole, quadrupole, and octupole transition probabilities, as well as the low-energy positive and negative-parity excitation spectra. Conversely, discrepancies between the spectroscopic data and the IBM results suggest that the mapping quality needs to be evaluated in order to determine if the mapped boson Hamiltonian or the fermionic calculations are the source of the issues.

Keywords

IBM, Energy Levels, Electromagnetic Octupole Transitions

1. Introduction

In the majority of medium-mass and heavy atomic nuclei, the ground state is characterized by quadrupole deformation and reflection symmetry. However, there are certain regions in the nuclear chart where the spatial reflection symmetry spontaneously breaks, leading to the emergence of octupole or pear-like deformations [1-3]. Specifically, atomic nuclei with neutron (N) and/or proton (Z) numbers close to the well-known "octupole magic" numbers of 34, 56, 88, and 134 are expected to display pronounced octupole correlations [1]. Examples of nuclei that exhibit significant octupole correlations are the neutron-rich lanthanides near $Z = 56$ and $N = 88$, as well as the light acti-

nides near $Z = 88$ and $N = 134$. In these nuclei, observable quantities such as low-lying negative-parity states and the intensities of electric dipole (E1) and octupole (E3) transitions are indicative of the presence of static ground-state octupole deformation. Currently, there is active experimental research focused on nuclear octupolarity. Several nuclei have already been identified as exhibiting distinct signatures of static ground-state octupole deformation [4-8].

From a theoretical standpoint, the investigation of octupole deformation has been approached using a diverse range of methods. These methods span from sophisticated microscopic

*Corresponding author: Saad.Abood@nahrainuniv.edu.iq (Saad Naji Abood)

Received: 12 January 2024; **Accepted:** 30 January 2024; **Published:** 28 April 2024



Copyright: © The Author(s), 2024. Published by Science Publishing Group. This is an **Open Access** article, distributed under the terms of the Creative Commons Attribution 4.0 License (<http://creativecommons.org/licenses/by/4.0/>), which permits unrestricted use, distribution and reproduction in any medium, provided the original work is properly cited.

calculations, which take into account the detailed interactions between individual nucleons, to macroscopic models that provide a more phenomenological description of the overall nuclear shape. Researchers employ these various theoretical approaches to gain insights into the nature and properties of octupole deformation in atomic nuclei.

Various computational methods have been utilized to explore octupole deformation in atomic nuclei. These include calculations based on geometrical collective models [9, 10], shell models [11, 12], interacting boson models (IBM) [13], self-consistent mean-field (SCMF) techniques with and without symmetry restoration [12-14], as well as cluster models [14, 15]. Each of these approaches offers unique insights into the nature and behavior of octupole deformation, contributing to our understanding of this phenomenon in nuclear systems. Noteworthy among the self-consistent mean-field (SCMF) approaches are the recent calculations that have been carried out to investigate octupole correlations in the low-lying states of nuclei around 144Ba. These calculations employ the full symmetry-restored (angular momentum, particle number, and parity) generator coordinate method (GCM) [16]. By incorporating these symmetries, the GCM approach provides a comprehensive framework for analyzing the octupole properties of these nuclei, yielding valuable insights into their structure and behavior. The aforementioned calculations utilize the Gogny [6, 17] and covariant EDF's [18] as their foundation. However, it is worth noting that performing full symmetry-projected generator coordinate method (GCM) calculations for heavy nuclear systems can be computationally demanding and time-consuming. As a result, alternative approaches are often employed to address the computational challenges associated with heavy nuclear systems. These include the utilization of alternative methods such as the full axial quadrupole-octupole two-dimensional GCM [19] or the collective Hamiltonian, which is an approximation to the GCM based on the Gaussian overlap approximation [20, 22]. These methods provide computationally more efficient ways to study octupole correlations in heavy nuclei while still capturing essential aspects of their structure and dynamics.

In this study, our focus is on investigating the spectroscopy of octupole and quadrupole collective states in lanthanide nuclei. Specifically, we concentrate on nuclei where the proton number $Z \approx 56$ and $N \approx 88$, as they are found in close proximity to the "octupole magic" numbers. To analyze the properties and behavior of these nuclei, we employ the Interacting Boson Model-1 (IBM-1). This model serves as a valuable tool for understanding the collective excitations and dynamics of atomic nuclei, allowing us to study the interplay between octupole and quadrupole effects in this particular region of the nuclear chart.

2. Interacting Boson Model (IBM)

From a microscopic viewpoint, the s, d, and f-bosons in the

IBM (Interacting Boson Model) framework can be understood as representing collective monopoles, quadrupoles, and octupoles, respectively. These bosons correspond to pairs of valence nucleons. In a specific nucleus, the total number of bosons, denoted as $N = n_s + n_d + n_f$, remains conserved and is equal to half the number of valence nucleons.

The proton-neutron Interacting Boson Model (IBM-2) provides a framework where theoretical distinctions between the degrees of freedom of protons and neutrons can be made [23, 24]. Nonetheless, the IBM-2 framework necessitates a substantial number of model parameters, especially when incorporating f-boson degrees of freedom. However, several phenomenological studies have successfully utilized the simpler sdf-IBM-1 framework, which does not differentiate between proton and neutron bosons. In our previous investigations of octupole correlations [25, 26], we employed the sdf-IBM-1 framework in this study to maintain consistency and to present our explanation in the simplest and most straightforward manner possible.

The identical sdf-IBM Hamiltonian utilized in our previous research on actinide nuclei [25, 26] has also been employed in this study.

$$H^{\wedge} = \varepsilon_d n_d^{\wedge} + \varepsilon_f n_f^{\wedge} + \kappa_2 Q_2^{\wedge} \cdot Q_2^{\wedge} + \rho L^{\wedge} \cdot L^{\wedge} + \kappa_3 Q_3^{\wedge} \cdot Q_3^{\wedge} \quad (1)$$

$$Q_2^{\wedge} = s^+ d^- + d^+ s^- + \chi_d (d^+ d^-)^{(2)} + \chi_f (f^+ f^-)^{(2)} \quad (2)$$

$$L^{\wedge} = \sqrt{10} (d^+ d^-)^{(1)} + \sqrt{28} (f^+ f^-)^{(1)} \quad (3)$$

$$Q_3^{\wedge} = s^+ f^- + f^+ s^- + \chi_3 (d^+ f^- + f^+ d^-)^{(3)} \quad (4)$$

It should be noted that in the $L^{\wedge} \cdot L^{\wedge}$ term, the term proportional to $(d^+ d^-)^{(1)} \cdot (f^+ f^-)^{(1)}$ have been overlooked [25]. For every nucleus, the parameters ε_d , ε_f , κ_2 , ρ , χ_d , χ_f , κ_3 , and χ_3 of the sdf-IBM Hamiltonian are chosen so that, in the boson condensate state, the expected value of the sdf-IBM Hamiltonian is in the vicinity of the global minimum [25, 27].

3. Results and Discussion

3.1. Energy Spectra

Figures 1 and 2 display the excitation spectra of the positive-parity even-spin and negative-parity odd-spin yrast states, respectively, obtained from our calculations for the Xe, Ba, Ce, and Nd nuclei. The excitation spectra of the positive-parity even-spin and negative-parity odd-spin yrast states for the Xe, Ba, Ce, and Nd nuclei are illustrated in Figures 1 and 2, respectively. These spectra were obtained through our calculations.

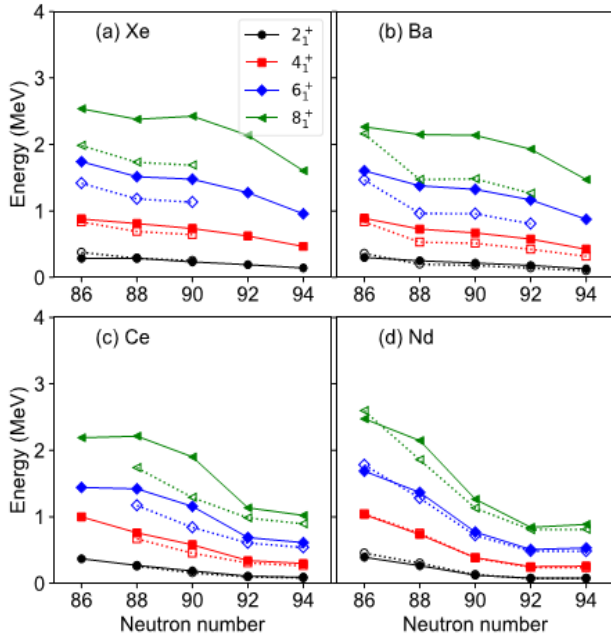


Figure 1. Displays, as functions of the neutron number, the low-energy excitation spectra of positive-parity even-spin yrast states in $^{140-148}\text{Xe}$, $^{142-150}\text{Ba}$, $^{144-152}\text{Ce}$, and $^{146-154}\text{Nd}$. These spectra were obtained by diagonalizing the mapped sdf-IBM Hamiltonian. The experimental data were obtained from Ref. [28].

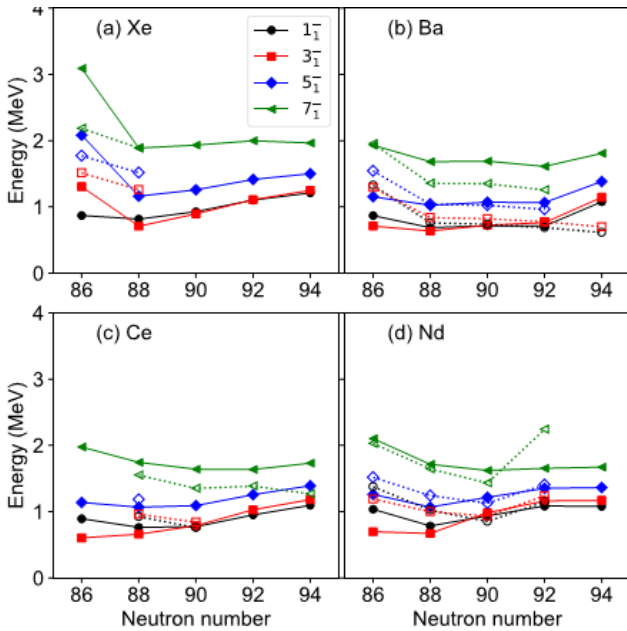


Figure 2. The same as in Figure 1 but for odd-spin negative-parity yrast states.

Both the sdf-IBM1 calculations and experimental data reveal a consistent decrease in the excitation energies of positive-parity yrast states as a function of neutron number, as depicted in Figure 1. This behavior is a characteristic feature of a shape transition from nearly spherical to deformed configurations. Empirical studies in references [29–31] have also considered the impact of shape phase transitions on posi-

tive-parity states in the neutron-rich Ba region. The findings demonstrate a notable structural change in the Ce and Nd isotopes around $N = 90$ and 92 . Remarkably, the positive-parity ground-state band obtained from the mapped IBM model exhibits a similar pattern when compared to experimental data. In quantitative terms, the majority of the studied nuclei with $N < 92$ exhibit a theoretical ground-state band that is considerably elongated, indicating a lower moment of inertia compared to the experimental data. This discrepancy is likely due to the mapping procedure, which determines an excessively high strength for the quadrupole-quadrupole interaction (κ_2).

The characteristic feature of octupole collectivity is the downward shift of low-lying negative-parity states relative to the positive-parity ground-state band. Figure 2 illustrates this pattern, which is observed in both the theoretical and experimental negative-parity values for each of the studied isotopic chains. As the neutron number approaches $N \approx 88$, the excitation energies of the expected negative-parity bands decrease. This neutron number corresponds to the point where the 3-excitation energy reaches its minimum value for most of the studied isotopic chains. However, as $N > 88$, the excitation energy of the negative-parity levels gradually increases. However, in the case of Ba isotopes, the excitation energies of the negative-parity states remain constant until $N = 92$. This indicates that Ba isotopes with neutron numbers ranging from 86 to 92 indeed possess an octupole-deformed ground state. Similar results are obtained for the Ce isotopes. In the case of Xe and Nd isotopes, the anticipated levels around $N = 88$ and 90 display a nearly parabolic pattern. This systematic behavior of the negative-parity states suggests a moderate evolution of octupole collectivity in the neutron-rich lanthanide region. However, when compared to experimental data, the predicted negative-parity bands for Ba and Xe isotopes consistently exhibit elongation. The underlying reason for this observation is the same as that discussed for the positive-parity states depicted in Figure 1.

Figure 3 depicts the excitation energies of the non-yrast states, specifically the 0_2^+ , 2_2^+ , and 4_2^+ levels. These states appear to form a quasi-beta band, where the 0 state acts as the bandhead for nuclei with $N > 90$. Notably, the computed energy levels exhibit an unconventional pattern for transitional nuclei with $N < 90$, as illustrated in Figure 3. In particular, the positions of the 0_2^+ and 2_2^+ energy levels are reversed, leading to an uneven band structure. This inversion results in significant level repulsion between low-spin states. Moreover, as depicted in Figures 3(c) and 3(d) for the highly quadrupole-deformed Ce and Nd isotopes, respectively, the calculated energy levels differ significantly from the observed ones. This discrepancy is a common characteristic of mapped IBM studies, primarily due to the unexpectedly high value of κ_2 observed ones. Indeed, this discrepancy between the calculated and observed energy levels is a common characteristic of mapped IBM research, primarily attributed to the

unexpectedly high value of κ_2 . Indeed, this discrepancy between the calculated and observed energy levels is a common characteristic of mapped IBM research, primarily attributed to the unexpectedly high value of κ_2 .

Figure 4 presents the excitation spectra of a distinct set of non-yrast states, specifically the 2_3^+ , 3_1^+ , 4_3^+ and 5_1^+ levels. According to the current calculations, these states are found to be associated with quasi- γ bands in the majority of the studied nuclei. As depicted in Figure 4, the energy levels exhibit a nearly harmonic pattern. However, it is worth noting that the 5_1^+ level stands out with a notably higher energy compared to the other levels in the band. This is especially prominent for lighter isotopes with lower neutron numbers. The experimental bandhead energy of the quasi-gamma band is significantly overestimated for the same reason as the quasi-beta band. In Figure 5, the expectation value of the f-boson number operator, derived from the IBM wave functions of the states (a) 0_1^+ , (b) 2_1^+ , (c) 0_2^+ , (d) 2_2^+ , (e) 1_1^- , and (f) 3_1^- , is plotted.

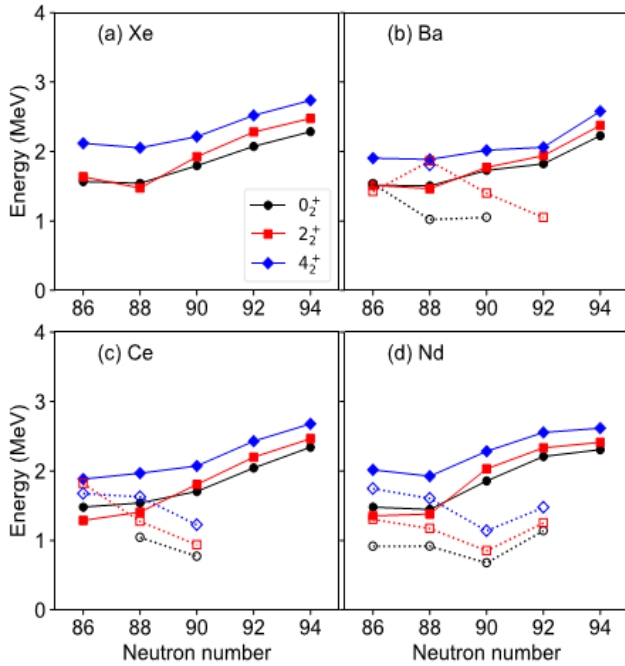


Figure 3. Identical to that shown in Figure 2, but for the states of 0_2^+ , 2_2^+ and 4_2^+ . The experimental data are derived from Refs. [28, 32].

A notable observation is that the wave functions of both the 0_1^+ and 2_1^+ states exhibit a substantial presence of f-boson components ($\langle n_f \rangle \approx 1$) at $N \approx 88$. This suggests that, for nuclei with $N \approx 88$, the octupole degree of freedom plays a vital role in shaping the low spin structure of the positive-parity ground-state bands.

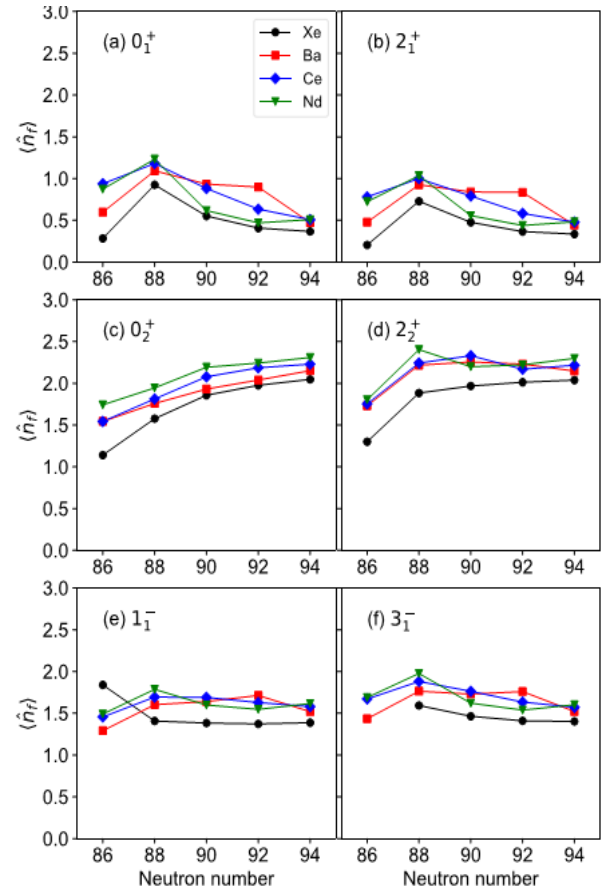


Figure 4. The expectation values of the f-boson number operator $\langle n_f \rangle$ in the IBM-1 wave functions corresponding to the states (a) 0_1^+ , (b) 2_1^+ , (c) 0_2^+ , (d) 2_2^+ , (e) 1_1^- , and (f) 3_1^- are plotted as functions of the neutron number.

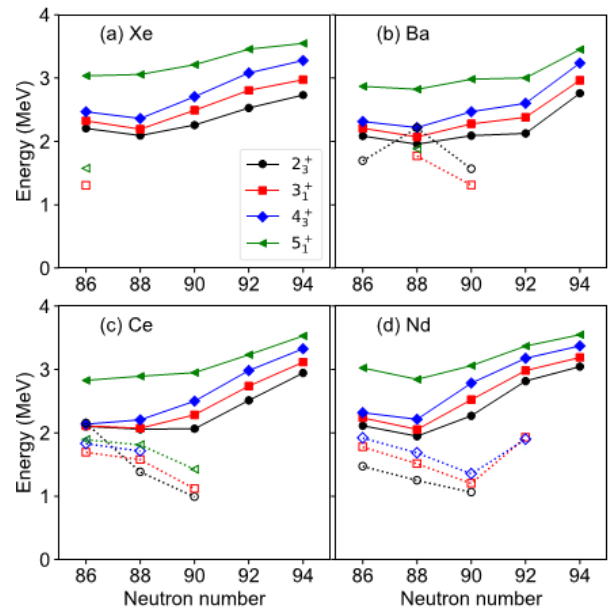


Figure 5. The low-energy excitation spectra of positive-parity even-spin yrast states in $^{140-148}\text{Xe}$, $^{142-150}\text{Ba}$, $^{144-152}\text{Ce}$ and $^{146-154}\text{Nd}$, computed by diagonalizing the mapped sdf-IBM are shown as functions of the neutron number. Experimental data have been taken from ref [28].

Except for the Xe isotopes, the $\langle n_f^\wedge \rangle \approx 2$ condition holds, indicating that the 0 state possesses a double octupole boson nature. Specifically, for $N \geq 88$, the f-boson content of the 2_2^+ state is comparable to that of the 0_2^+ state. Additionally, the wave functions of the 1_1^- and 3_1^- states exhibit f bosons within the $1 \leq \langle n_f^\wedge \rangle \leq 2$ range.

$$T^\wedge(E1) = e_1 (d^+ f^- + f^+ d^-)^{(1)} \quad (5)$$

$$T^\wedge(E2) = e_2 Q_2^\wedge = e_2 [s^+ d^- + d^+ s^- + \chi_d (d^+ d^-)^{(2)} + \chi_f (f^+ f^-)^{(2)}] \quad (6)$$

$$T^\wedge(E3) = e_3 Q_3^\wedge = e_3 [s^+ f^- + f^+ s^- + \chi_3 (d^+ f^- + f^+ d^-)^{(3)}] \quad (7)$$

In order to reasonably duplicate the experimental $B(E2; 1_1^- \rightarrow 0_1^+)$ and $B(E2; 2_1^+ \rightarrow 0_1^+)$ transition probabilities, the boson effective charges $e_1 = 0.02 \sqrt{eb}$ and $e_2 = 0.17 \text{ eb}$ are fixed. Nonetheless, the significant $B(E2; 3_1^- \rightarrow 0_1^+)$ values seen experimentally in those nuclei with elevated octupole correlations must be taken into account in order to fix e_3 .

In Table 1, the reduced transition probabilities calculations are compared with the experimental results [5, 6, 28, 33]. There is good agreement between the experimental and B(E1) and B(E2) rates. Beyond $N = 88-90$, they exhibit a sharp increase that is compatible with the emergence of substantial collectivity. Furthermore, $N = 88$ corresponds to the maximum B(E3) rate for each isotopic chain. Additionally, there is a fair amount of agreement between the computed and experimental B(E3) values. Specifically, the estimated B(E3) rates for $^{144,146}\text{Ba}$ fall within the experimental error ranges [5, 6].

Table 1. The IBM-1 calculations for B(E1), B(E2) and B(E3) transitions (in W. U) compared with experimental data [5, 6] in Ba and Nd nuclei.

Nuclei	E λ	transitions	Exp.	IBM-1
^{144}Ba	E2	$2_1^+ \rightarrow 0_1^+$	48_{-2}^{+2}	42
		$4_1^+ \rightarrow 2_1^+$	86_{-7}^{+10}	78
		$6_1^+ \rightarrow 4_1^+$	54_{-6}^{+7}	52
		$8_1^+ \rightarrow 6_1^+$	55_{-12}^{+19}	55.5
	E3	$3_1^- \rightarrow 0_1^+$	48_{-34}^{+25}	51
		$5_1^- \rightarrow 0_1^+$	< 103	90
		$7_1^- \rightarrow 4_1^+$	< 135	121

3.2. Electric Transition Probability

The electric dipole, quadrupole, and octupole transition operators $T^\wedge(E\lambda)$ ($\lambda = 1, 2, 3$) are used to calculate transition probabilities. They are defined as follows [25, 26]:

Nuclei	E λ	transitions	Exp.	IBM-1
^{146}Ba	E1	$1_1^- \rightarrow 0_1^+$	$9.3_{-0.7}^{+0.8} \times 10^{-7}$	11
		$1_1^- \rightarrow 2_1^+$	$(6.6 \pm 0.5) \times 10^{-6}$	6.2
		$3_1^- \rightarrow 4_1^+$	$(1.59 \pm 0.09) \times 10^{-5}$	1.88
		$3_1^- \rightarrow 2_1^+$	$(1.84 \pm 0.13) \times 10^{-6}$	1.96
		$2_1^+ \rightarrow 0_1^+$	60 ± 2	67
	E2	$4_1^+ \rightarrow 2_1^+$	94 ± 21	102
		$6_1^+ \rightarrow 4_1^+$	93_{-27}^{+23}	89
		$8_1^+ \rightarrow 6_1^+$	61_{-24}^{+48}	59
		$3_1^- \rightarrow 1_1^-$	45 ± 38	48
		$3_1^- \rightarrow 0_1^+$	48_{-29}^{+23}	55
	E3	$5_1^- \rightarrow 0_1^+$	73_{-29}^{+88}	70
		$7_1^- \rightarrow 4_1^+$	82_{-45}^{+112}	80
		$9_1^- \rightarrow 6_1^+$	94_{-94}^{+100}	102
		$5_1^- \rightarrow 4_1^+$	0.00205 ± 0.0021	0.030
^{148}Nd	E1	$7_1^- \rightarrow 6_1^+$	0.0043 ± 0.0010	0.055
		$8_1^+ \rightarrow 7_1^-$	0.0049 ± 0.0011	0.043
	E2	$2_1^+ \rightarrow 0_1^+$	57.9 ± 2.2	53.8
		$4_1^+ \rightarrow 2_1^+$	94 ± 4	98.3
		$0_2^+ \rightarrow 2_1^+$	31.2 ± 2.2	33.0
		$2_2^+ \rightarrow 0_1^+$	0.54 ± 0.08	0.62

Nuclei	E λ	transitions	Exp.	IBM-1
		$2_2^+ \rightarrow 2_1^+$	14.4 ± 1.9	16.2
		$2_2^+ \rightarrow 4_1^+$	16 ± 8	18
		$2_3^+ \rightarrow 0_1^+$	1.4 ± 0.4	2.72
		$6_1^+ \rightarrow 4_1^+$	102 ± 7	105
		$8_1^+ \rightarrow 6_1^+$	98 ± 17	
		$7_1^- \rightarrow 5_1^-$	$(1.5 \pm 0.6) \times 10^2$	
E3		$3_1^- \rightarrow 0_1^+$	34 ± 3	

4. Conclusion

The findings of this study on neutron-rich lanthanide nuclei, combined with previous research on rare-earth [27] and light actinide nuclei [28, 29], indicate that the octupole degree of freedom plays a vital role in understanding the spectroscopic properties and structural evolution of low-lying states in specific regions of the nuclear chart. These results suggest that the octupole degree of freedom is a fundamental aspect contributing to the overall nuclear structure and behavior in certain regions of the nuclear landscape. The sdf-IBM framework provides a plausible explanation for significant spectroscopic features that help elucidate the interplay between the octupole and quadrupole degrees of freedom in the studied region. The obtained results from the current analysis serve as a motivation to explore the applicability of octupole deformations in other mass regions. Specifically, proton-rich nuclei with $Z \approx N \approx 56$ appear to be promising candidates for further investigation. Ongoing research in this direction will delve into these nuclei and their spectroscopic characteristics, and the findings will be presented in an upcoming article.

Several recommendations are made in this regard:

The computational results in this study may have overestimated the excitation energies of the 6_1^+ and 8_1^+ states in Xe and Ba isotopes. This can be attributed to the occupancy of $f_{7/2}$ ($g_{7/2}$) orbitals by neutrons (protons) in this region, which form nucleon pairs with $J = 6^+$. The inclusion of the equivalent i-boson in the IBM framework may lead to a lowering of the energy of these yrast states with $I \geq 6$, providing a more accurate description of their spectroscopic properties.

The systematic behavior of the 7^- state energy in Ba and Nd isotopes could not be accurately reproduced by the IBM, as evident from the obtained results. To gain further insights, it would be valuable to investigate whether the empirical trend of this state can be replicated through fermionic calculations within the sdf-IBM framework. Performing such calculations can provide a more comprehensive understanding of the underlying physics and help bridge the gap between experi-

mental observations and theoretical predictions for the 7^- state in these isotopes.

The IBM framework was unable to accurately reproduce the systematic behavior of the 7^- energy in Ba and Nd isotopes, as evidenced by the results. To further explore this phenomenon, it would be valuable to investigate whether the empirical trend of this state can be replicated using fermionic calculations within the sdf-IBM framework. By employing fermionic calculations, researchers can delve deeper into the underlying physics and determine if incorporating additional fermionic degrees of freedom can better capture the observed empirical trend of the 7^- state in Ba and Nd isotopes. This investigation can provide valuable insights into the nuclear structure and shed light on the interplay between collective and single-particle degrees of freedom.

The results of the study revealed that the quasi-beta and quasi-gamma bands obtained from the calculations were considerably higher in energy compared to the corresponding bands observed in experimental measurements. This discrepancy suggests that the theoretical model used in the study may not fully capture all the relevant physics and interactions responsible for the observed spectroscopic properties. Further investigations and refinements of the theoretical framework are necessary to better understand and reproduce the experimental observations of these bands. This could involve considering additional degrees of freedom, refining the parameters of the model, or exploring alternative theoretical approaches to improve the agreement between theory and experiment.

Conflicts of Interest

The authors declare no conflicts of interest.

References

- [1] P. A. Butler and W. Nazarewicz, *Rev. Mod. Phys.* 68 (1996) 349.
- [2] P. A. Butler, *J. Phys. G: Nucl. Part. Phys.* 43 (2016) 073002.
- [3] P. A. Butler, *Proc. Roy. Soc. A: Mathematical, Physical and Engineering Sciences* 476 (2020) 0200202.
- [4] L. P. Gaffney, P. A. Butler, M. Scheck, A. B. Hayes, F. Wenander, M. Albers, B. Bastin, C. Bauer, A. Blazhev, S. Bönig, N. Bree, J. Cederkäll, T. Chupp, D. Cline, T. E. Colosios, T. Davinson, H. D. Witte, J. Diriken, T. Grahn, A. Herzan, M. Huyse, D. G. Jenkins, D. T. Joss, N. Kesteloot, J. Konki, M. Kowalczyk, T. Kröll, E. Kwan, R. Lutter, K. Moschner, P. Napiorkowski, J. Pakarinen, M. Pfeiffer, D. Radeck, P. Reiter, K. Reynders, S. V. Rigby, L. M. Robledo, M. Rudigier, S. Sami, M. Seidlitz, B. Siebeck, T. Stora, P. Thoele, P. V. Duppen, M. J. Vermeulen, M. von Schmid, D. Voulot, N. Warr, K. Wimmer, K. WrzosekLipska, C. Y. Wu, and M. Zielinska, *Nature (London)* 497 (2013) 199.

- [5] B. Bucher, S. Zhu, C. Y. Wu, R. V. F. Janssens, D. Cline, A. B. Hayes, M. Albers, A. D. Ayangeakaa, P. A. Butler, C. M. Campbell, M. P. Carpenter, C. J. Chiara, J. A. Clark, H. L. Crawford, M. Cromaz, H. M. David, C. Dickerson, E. T. Gregor, J. Harker, C. R. Hoffman, B. P. Kay, F. G. Kondev, A. Korichi, T. Lauritsen, A. O. Macchiavelli, R. C. Pardo, A. Richard, M. A. Riley, G. Savard, M. Scheck, D. Seweryniak, M. K. Smith, R. Vondrasek, and A. Wiens, *Phys. Rev. Lett.* 116 (2016) 112503.
- [6] B. Bucher, S. Zhu, C. Y. Wu, R. V. F. Janssens, R. N. Bernard, L. M. Robledo, T. R. Rodríguez, D. Cline, A. B. Hayes, A. D. Ayangeakaa, M. Q. Buckner, C. M. Campbell, M. P. Carpenter, J. A. Clark, H. L. Crawford, H. M. David, C. Dickerson, J. Harker, C. R. Hoffman, B. P. Kay, F. G. Kondev, T. Lauritsen, A. O. Macchiavelli, R. C. Pardo, G. Savard, D. Seweryniak, and R. Vondrasek, *Phys. Rev. Lett.* 118 (2017) 152504.
- [7] P. A. Butler, L. P. Gaffney, P. Spagnoletti, K. Abrahams, M. Bowry, J. Cederkäll, G. de Angelis, H. De Witte, P. E. Garrett, A. Goldkuhle, C. Henrich, A. Illana, K. Johnston, D. T. Joss, J. M. Keatings, N. A. Kelly, M. Komorowska, J. Konkki, T. Kroll, M. Lozano, B. S. Nara Singh, D. O'Donnell, J. Ojala, R. D. Page, L. G. Pedersen, C. Raison, P. Reiter, J. A. Rodriguez, D. Rosiak, S. Rothe, M. Scheck, M. Seidlitz, T. M. Shneidman, B. Siebeck, J. Sinclair, J. F. Smith, M. Stryczyk, P. Van Duppen, S. Vinals, V. Virtanen, N. Warr, K. Wrzosek-Lipska, and M. Zielińska, *Phys. Rev. Lett.* 124 (2020) 042503.
- [8] M. M. R. Chishti, D. O'Donnell, G. Battaglia, M. Bowry, D. A. Jaroszynski, B. S. N. Singh, M. Scheck, P. Spagnoletti, and J. F. Smith, *Nat. Phys.* 16 (2022) 853.
- [9] D. Bonatsos, D. Lenis, N. Minkov, D. Petrellis, and P. Yotov, *Phys. Rev. C* 71 (2023) 064309.
- [10] P. G. Bizzeti and A. M. Bizzeti-Sona, *Phys. Rev. C* 88 (2013) 011305.
- [11] N. Yoshinaga, K. Yanase, K. Higashiyama and E. Teruya, *Phys. Rev. C* 98 (2018) 044321.
- [12] N. Yoshinaga, K. Yanase, C. Watanabe, and K. Higashiyama, *Prog. Theor. Exp. Phys.* 221 (2021) 063D01.
- [13] O. Vallejos and J. Barea, *Phys. Rev. C* 104 (2021) 014308.
- [14] T. M. Shneidman, G. G. Adamian, N. V. Antonenko, R. V. Jolos, and W. Scheid, *Phys. Lett. B* 526 (2002) 322.
- [15] T. M. Shneidman, G. G. Adamian, N. V. Antonenko, R. V. Jolos, and W. Scheid, *Phys. Rev. C* 67 (2003) 014313.
- [16] P. Ring and P. Schuck, *The nuclear many-body problem*, (Berlin: Springer-Verlag, 1980).
- [17] R. Ličá, G. Benzoni, T. R. Rodríguez, M. J. G. Borge, L. M. Fraile, H. Mach, A. I. Morales, M. Madurga, C. O. Sotty, V. Vedia, H. De Witte, J. Benito, R. N. Bernard, T. Berry, A. Bracco, F. Camera, S. Ceruti, V. Charviakova, N. Cieplicka-Oryńczak, C. Costache, F. C. L. Crespi, J. Creswell, G. Fernandez-Martínez, H. Fynbo, P. T. Greenlees, I. Hogg, M. Huyse, J. Jolie, V. Karayonchev, U. Köster, J. Konkki, T. Kroll, J. Kurcewicz, T. Kurtukian-Nieto, I. Lazarus, M. V. Lund, N. Marginean, R. Marginean, C. Mihai, R. E. Mihai, A. Negret, A. Orduz, Z. Patyk, S. Pascu, V. Pucknell, P. Rahkila, E. Rapisarda, J. M. Regis, L. M. Robledo, F. Rotaru, N. Saed-Samii, V. Sánchez-Tembleque, M. Stanoiu, O. Tengblad, M. Thuerauf, A. Turturica, P. Van Duppen, and N. Warr (IDS Collaboration), *Phys. Rev. C* 97 (2018) 024305.
- [18] Y. Fu, H. Wang, L.-J. Wang, and J. M. Yao, *Phys. Rev. C* 97 (2018) 024338.
- [19] L. M. Robledo and P. A. Butler, *Phys. Rev. C* 88 (2013) 051302.
- [20] L. M. Robledo, J. L. Egido, B. Nerlo-Pomorska, and K. Pomorski, *Phys. Lett. B* 201 (1998) 409.
- [21] S. Y. Xia, H. Tao, Y. Lu, Z. P. Li, T. Nikšić, and D. Vretenar, *Phys. Rev. C* 96, 054303 (2017).
- [22] K. Nomura, L. Lotina, T. Nikšić, and D. Vretenar, *Phys. Rev. C* 103 (2021), 054301.
- [23] T. Otsuka, A. Arima, and F. Iachello, *Nucl. Phys. A* 309 (1978) 1.
- [24] T. Mizusaki and T. Otsuka, *Prog. Theor. Phys. Suppl.* 125 (1996) 97.
- [25] K. Nomura, R. Rodríguez-Guzmán, Y. M. Humadi, L. M. Robledo, and J. E. García-Ramos, *Phys. Rev. C* 102 (2020) 064326.
- [26] K. Nomura, R. Rodríguez-Guzmán, L. M. Robledo, and J. E. García-Ramos, *Phys. Rev. C* 103 (2021) 044311.
- [27] K. Nomura, R. Rodríguez-Guzmán, and L. M. Robledo, *Phys. Rev. C* 92 (2015) 014312.
- [28] Brookhaven National Nuclear Data Center, <http://www.nndc.bnl.gov>
- [29] M. Sugawara and H. Kusakari, *Phys. Rev. C* 75, 067302 (2007).
- [30] J. B. Gupta and M. Saxena, *Phys. Rev. C* 91, 054312 (2015).
- [31] S. Y. Lee, J. H. Lee, and Y. J. Lee, *J. Korean Phys. Soc.* 72, 1147 (2018).
- [32] S. J. Zhu, E. H. Wang, J. H. Hamilton, A. V. Ramayya, Y. X. Liu, N. T. Brewer, Y. X. Luo, J. O. Rasmussen, Z. G. Xiao, Y. Huang, G. M. Ter-Akopian, and T. Oganessian, *Phys. Rev. Lett.* 124 (2020) 032501.
- [33] T. Kibedi and R. Spear, *Atomic Data and Nuclear Data Tables* 80 (2002) 35.